Clim. Past Discuss., 8, 2281–2320, 2012
www.clim-past-discuss.net/8/2281/2012/
doi:10.5194/cpd-8-2281-2012

Climate of the Past Discussions

Holocene climate variability in the winter rainfall zone of South Africa

S. Weldeab[1], J.-B. W. Stuut[2,3], R. R. Schneider[4], and W. Siebel[5]

[1]Department of Earth Science, University of California, Santa Barbara, CA 93106-9630, USA
[2]NIOZ, Royal Netherlands Institute for Sea Research, Texel, The Netherlands
[3]MARUM, Center for Marine Environmental Sciences, University of Bremen, Bremen, Germany
[4]Institute of Geosciences, University of Kiel, Kiel, Germany
[5]Department of Geosciences, University of Tübingen, Tübingen, Germany

Received: 16 May 2012 – Accepted: 4 June 2012 – Published: 18 June 2012

Correspondence to: S. Weldeab (weldeab@geol.ucsb.edu)

Published by Copernicus Publications on behalf of the European Geosciences Union.

Abstract

We established a multi-proxy time series comprising analyses of major elements in bulk sediments, Sr and Nd isotopes, grain size of terrigenous fraction, and $\delta^{18}O$ and $\delta^{13}C$ in tests of *Neogloboquadrina pachyderma* (sinistral) from a marine sediment sequence recovered off the Orange River. The records reveal coherent patterns of variability that reflect changes in wind strength, precipitation over the river catchments, and upwelling of cold and nutrient-rich coastal waters off Western South Africa. The wettest episode of the Holocene in the Winter Rainfall Zone (WRZ) of South Africa occurred during the "Little Ice Age" (700–100 yr BP). Wet phases were accompanied by strengthened coastal water upwellings, a decrease of Agulhas water leakage into the Southern Atlantic, and a reduced dust incursion over Antarctica. A continuous aridification trend in the WRZ and a weakening of the Southern Benguela Upwelling System (BUS) between 9000 and 5500 yr BP parallel with evidence of a poleward shift of the austral mid-latitude westerlies and an enhanced leakage of warm Agulhas water into the Southeastern Atlantic. The temporal relationship between precipitation changes in the WRZ, the thermal state of the coastal surface water, and variation of dust incursion over Antarctica suggests a causal link that most likely was related to latitudinal shifts of the Southern Hemisphere westerlies and changes in the amount of Agulhas water leakage into the Southern BUS. Our results of the mid-Holocene time interval may serve as an analogue to a possible long-term consequence of the current and future southward shift of the westerlies that may result in a decline of rainfall over Southwest Africa and a weakened upwelling with implication for phytoplankton productivity and fish stocks. Furthermore, warming of the coastal surface water as a result of warm Agulhas water incursion into the Southern BUS may affect coastal fog formation that is critical as moisture source for the endemic flora of the Namaqualand.

CPD
8, 2281–2320, 2012

1 Introduction

Instrumental and modeling data indicate that the southward displacement of austral westerlies and increased amount of leakage of warm, saline Agulhas water into the Southern Atlantic may have a negative impact on the Winter Rainfall Zone (WRZ) of South Africa and weakens the Southern BUS (Biastoch et al., 2008, 2009; Lutjeharms et al., 2001; MacKellar et al., 2007; Hardman-Mountford et al., 2003). Paleoclimate records can provide insights that may help to assessing the long-term impact of such ocean-atmosphere changes. However, conventional terrestrial climate archives such as lake and cave deposits are sparse in arid and semi-arid regions, limiting a dense spatio-temporal coverage and multi-proxy approach of climate reconstructions, a pre-requisite to gain a better understanding of regional climate variability and its link to large-scale atmosphere–ocean climate coupling. The coastal area of Southwest Africa is located in the semi-arid ecosystems (MacKellar et al., 2007 and reference therein), and our knowledge of past climate variability so far relied on a few low-resolved proxy records. The emergence of new climate archives and proxies such as hyrax dung and optically stimulated luminescence dating have led to relatively more spatio-temporal coverage of paleoclimate information for the Southwest Africa (Chase et al., 2009, 2011; Chase and Thomas, 2006, 2007; Meadows et al., 2010; Meadows and Sugden, 1991; Scott and Woodborne, 2007a, b). These records and along with the most recent high resolution climate reconstruction of the Late Holocene from the western coastal area of South Africa (Benito et al., 2011; Stager et al., 2012) reveal that the WRZ of South Africa was very sensitive to centennial- and millennial-scale climate oscillations during the Holocene epoch. Notwithstanding the increasing number of paleo-records, the regional significance of and temporal correlation between the local climate signals and their link to surface water conditions of the adjacent ocean remain uncertain. Our study adds to the emerging pattern of past climate variability in Southwest Africa by providing a spatially integrated record of terrestrial climate changes and its link to adjacent coastal water conditions that allow to infer possible climatic links to the Southern

Hemisphere westerlies and the leakage of warm Agulhas water into the Southeastern Atlantic.

2 Regional setting

The Winter Rainfall Zone (WRZ) of Southwestern Africa stretches along the Southeastern Atlantic coastal region from Southwestern Namibia to Cape Agulhas and extends inland to the western margin of the Great Escarpment (Chase and Meadows, 2007; MacKellar et al., 2007) (Fig. 1). The WRZ receives >65 % of the annual rainfall during the austral winter, and consists of arid and semi-arid region including the Southern Namib Desert and the Namaqualand of South Africa (Chase and Meadows, 2007; MacKellar et al., 2007; Cowling et al., 1999). Along the coastal area, precipitation varies between 50 mm and 350 mm per year with strong local patterns (MacKellar et al., 2007).

We focus on a marine sediment sequence recovered from the mudbelt whose detrital composition is determined by fluvial and eolian sediment inputs from the Orange River, the Namaqualand, and the Namib and Kalahari deserts. The mudbelt is a prominent Holocene sediment package that covers a narrow strip along the inner-shelf between the Kunene River in the northwest and St. Helena Bay in the southeast (Compton et al., 2009, 2010; Herbert and Compton, 2007; Meadows et al., 2002; Rogers and Rau, 2006). Within the mudbelt, grain size distributions of terrigenous sediments are controlled by surface and subsurface currents as well as wave activities (Meadows et al., 2002; Rogers and Rau, 2006). A southeasterly surface current carries the sandy fraction of the fluvial sediment to the northwest of the Orange River. Northwesterly undercurrents distribute clayey-silty material to the southeast of the Orange River mouth, with decreasing grain size toward the southeastern end of the mudbelt (Meadows et al., 2002; Rogers and Rau, 2006). Hydrographic conditions in the coastal area are characterized by inner-shelf upwelling and the planktonic foraminiferal assemblage is dominated by *Neogloboquadrina pachyderma* (sinistral) (Rogers and Rau, 2006).

CPD
8, 2281–2320, 2012

On average, sea surface temperature and salinity account for 13.5 °C and 35 practical salinity unit (psu) during the austral winter and 16.9 °C and 34.9 psu during the austral summer (Locarnini et al., 2010). In the Southern BUS, sea surface temperature and nutrient availability is controlled by southeasterly wind-induced upwellings of cold and nutrient-rich waters. The upwelling prevails throughout the year with enhanced intensity during the austral winter. Within the Southern BUS, localized cells of strong upwelling exist including the Namaqua cell (Hardman-Mountford et al., 2003) from which the GeoB8332-4 was recovered. On interannual and interdecadal time scales, a weakening of the Southern BUS occurs in response to a southward shift the austral westerlies that allows the intrusion of warm Agulhas surface water into the Southeastern Atlantic (Hardman-Mountford et al., 2003; Biastoch et al., 2009).

The Orange River presents the most dominant sediment source for the mudbelt with 60 million metric $t\,yr^{-1}$ delivery of sediment and a relatively small volume of runoff ($11\,km^3\,yr^{-1}$) (Bremner et al., 1990). Most of the Orange River runoff and suspended sediment comes from the easternmost catchment that receives annual rainfall between 500 mm and >750 mm (Compton et al., 2010) (Fig. 1). Detailed mineralogical, chemical, and isotopic evidence indicate that the suspended sediments of Orange River mainly originate from the upper part of Karoo Supergroup (Late Triassic continental sedimentary rocks) (Compton and Maake, 2007; de Villiers et al., 2000). The Drakenberg Plateau, which is composed of flood basalt intersected by dolerite dykes/sills, receives high precipitation (>750 $mm\,yr^{-1}$), but contributes relatively small amounts to the total sediment load of the Orange River (Compton and Maake, 2007; de Villiers et al., 2000).

Holgat, Buffels, and Olifants rivers drain the western coastal area of South Africa (Fig. 1) that consists of Precambrian sedimentary rocks (>2.5 billion yr (Ga) old) that were intruded by 1 Ga old granite and gneiss (Cowling et al., 1999). Riverine and eolian sediment inputs from the coastal area (Herbert and Compton, 2007; Meadows et al., 2002; Rogers and Rau, 2006) as well as dust originating from the Namib Desert contribute a significant amount of sediment to the mudbelt (Prospero et al., 2002). We

CPD
8, 2281–2320, 2012

investigated the temporal variation of the sediment input from those various sources and obtained a detailed account of regional Holocene climate variability.

3 Material and methods

Our study focuses on sediment core GeoB8332-4 recovered within the mudbelt (29°07.66′ S, 16°39.57′ E, water depth 117 m), approximately 10 km and 40 km off the Holgat and Orange rivers, respectively (Fig. 1). The down core measurements are complemented by analysis of sediments collected from river-beds and suspended sediment of the Orange River and local Holgat, Buffels, and Olifants rivers (Fig. 1). The GeoB8332-4 sediment sequence consists of a monotonous dark greenish-gray mud that is slightly bioturbated and had a strong H_2S odor at time of the recovery. On-board measurements of color reflectance, magnetic susceptibility, porosity, and wet bulk density show also a monotonous trend (Schneider et al., 2003). The GeoB8332-4 core terminates at a sediment depth of 808 cm with a sediment layer that is rich in gastropod and bivalve shells. Throughout the sediment sequence, several intact and well-preserved shells of small gastropods and bivalves were found. Due to the low abundance of foraminifera we used gastropod shells for ^{14}C dating.

The age model of GeoB8332-4 sediment is based on 15 radiocarbon datings of small well-preserved gastropod shells (*Nassarius vinctus,* personal communication with John Compton, 2004). Prior to the selection for ^{14}C dating, the gastropod shells were carefully inspected for signs of corrosion and fragmentation that could be indicative for transport by waves and currents. To our best judgment, the gastropods we used for dating are autochthonous. The absence of age reversals in the densely dated sections and replicated measurements support the autochthonous origin of the gastropod samples (Fig. 2 and Table 1). Radiocarbon measurements were conducted at the Leibniz Institute for Radiometric Dating and Isotope Research in Kiel, Germany. The ^{14}C data reveal that the GeoB8332-4 sediment sequence contains a highly resolved climate record of the Early to Middle Holocene (11 500–5000 cal yr BP) and the last 700 yr

BP. Unfortunately, a hiatus covers the interval between 5000 and 700 yr BP. Nonetheless, the late and early-middle Holocene record provides detailed insights into climate variability of Southwestern Africa. The ^{14}C data were converted to calendar ages using CALIB software (Stuiver and Reimer, 1993) (version 6.10), Marine data set 2009 (Reimer et al., 2009), and ΔR of 129 ± 19 yr reservoir age of the local coastal water (Reimer et al., 2009). The final age model is established using polynomial (11 500–5000 yr BP) and linear (700–0 yr BP) equations describing the relationship between sediment depth and calendar ages (Fig. 2).

Prior the grain-size analysis of terrigenous fraction, we removed the biogenic fraction from GeoB8332-4 sediment samples. Organic matter and carbonate components were removed by adding 10 ml of H_2O_2 (35 %) and 100 ml HCl (1 %) to 750 mg of bulk sediment and boiling for one minute, respectively. Following the carbonate dissolution reaction, neutral pH was achieved by dilution with de-ionized water. As a final pre-treatment step, biogenic silica was removed. Six grams of NaOH pellets dissolved in 100 ml de-ionized water were added to the sediment and the mixture was boiled for 10 min. The solution was diluted with de-ionized water to neutral pH. Prior to grain-size analysis, the remaining terrigenous fraction was boiled with 300 mg of soluble sodium pyrophosphate ($Na_4P_2O_7 \cdot 10\,H_2O$) to foster particle disaggregation. Grain-size analysis was performed using a Coulter laser particle sizer LS200. The analysis resulted in 92 size classes varying from 0.39 to 2000 µm. An end-member modeling algorithm was applied to determine the proportions of distinct sediment components contributing to the measured particle size signal (Weltje, 1997; Stuut et al., 2002) (Fig. 3a–e). The algorithm output is a series of models, each containing a different number of "end-members", and each model explaining a different amount of variance. The higher the number of end-members the more variance is explained (Fig. 3d). Two key parameters are used to determine the minimum number of end-members required for a satisfactory approximation of the measured data (Prins et al., 2000; Stuut et al., 2002; Weltje, 1997). First, the coefficient of determination per size class (r^2) is used to assess how well the model reproduces the data in each size class (Fig. 3c). Second, the mean

CPD
8, 2281–2320, 2012

Holocene climate variability in the winter rainfall zone of South Africa

S. Weldeab et. al.

coefficient of determination (r^2_{mean}) averaged for all size classes is used to test how well each model reproduces the average of all measured size classes (Fig. 3d). In this study, the model with a minimum number of 3 end-members (EM1, EM2, and EM3), with $r^2 > 0.5$ and r^2_{mean} equal to 0.79 represents the best compromise (Fig. 3).

Time series of major element intensities were generated at 1 cm sampling interval using the Aavatech XRF Scanner I at the University of Bremen. The Core Scanner was run with an excitation potential of 10 kV, a current of 250 µA, and 30 s counting time. Element intensities were normalized by dividing the total counts for each element by the sum of total counts for all measured elements. In this study we focus only on Ca/Al, K/Al and Ti/Al ratios (Fig. 4).

Analysis of $\delta^{18}O$ and $\delta^{13}C$ in tests of *Neogloboquadrina pachyderma* (sinistral) (125–300 µm) from down core samples were performed with a Thermo MAT 253 mass spectrometer at the first author's stable isotope lab at UCSB. The mass spectrometer is coupled online to a Kiel IV Carbonate Device for automated CO_2 preparation. Samples were reacted by automated individual phosphoric acid addition. Results were corrected using NBS19 standard and are reported on the Peedee Belemnite (PDB) scale. Estimates for standard error (2σ) in the $\delta^{18}O$ and $\delta^{13}C$ measurements are better than ±0.07 ‰ and ±0.03 ‰, respectively.

Analyses of the $^{87}Sr/^{86}Sr$ and $^{143}Nd/^{144}Nd$ ratios on the lithogenic fraction (≤120 µm) of marine and riverine sediments were conducted on a Finnigan MAT 262 mass spectrometer using static collection mode at the Institute of Geosciences, University of Tübingen. In order to remove the carbonate fractions of down core samples, 500 mg of sediment was leached with 10 ml acetic acid (5 M) at room temperature for 12 h. The detrital residual were rinsed four times with ultrapure water, centrifuged, and the supernatant was removed. A 50-mg portion of the powdered and homogenized lithogenic fraction was spiked with a mixed ^{149}Sm:^{150}Nd spike prior to digestion in HF. The digested samples were dried and dissolved in 6 N HCl, dried and then redissolved in 2.5 N HCl. Analyses of NBS-SRM 987 and La Jolla Nd standards during this study yielded an average value of $^{87}Sr/^{86}Sr$=0.710244 ± 15

CPD
8, 2281–2320, 2012

and for $^{143}Nd/^{144}Nd=0.511823 \pm 15$, respectively. $^{87}Sr/^{86}Sr$ ratios are normalized to $^{86}Sr/^{88}Sr=0.1194$ and the $^{143}Nd/^{144}Nd$ ratios to $^{146}Nd/^{144}Nd=0.7219$. Results of Nd and Sr in blank measurements are 80 pg and 65 pg, respectively. The $^{143}Nd/^{144}Nd$ ratios are expressed as εNd, where εNd is the analyzed $^{143}Nd/^{144}Nd$ ratio normalized to the "chondritic uniform reservoir" value of 0.512638 (Jacobson and Wasserburg, 1980).

4 Results

4.1 Variations of terrigenous particle size

The particle size frequency distribution shows a bi-modal distribution pattern (Fig. 3a). The time series of the median grain size is marked by a continuous increase of particle size from the early to middle Holocene and declining trends between 5500 and 5000 yr BP as well as during the last 700 yr (Fig. 3b). We used an end-member modeling technique to narrow down the number of dominant end-members to three that sufficiently explain the variability of the median grain size throughout the investigated time intervals (Fig. 3b, e). End-member 3 (EM3) has a modal grain size value of ∼5 µm and its temporal variability is characterized by a continuous decline from the early to middle Holocene (Fig. 3b). In contrast, the fraction of EM3 shows a continuous increase over the last 700 yr BP, explaining up to 90 % of the median grain size variability. Pronounced changes in EM2 with a modal value of ∼10 µm are most evident between 7500 and 5500 yr BP and between 400 and 150 yr BP, both periods characterized by a decrease in medium grain size. The modal grain size of EM1 is ∼20 µm and reveals a large increase between 9250 and 6500 yr BP, followed by a sharp decline between 5500 and 5000 yr BP and 700 and 150 yr BP. Comparing the trends and magnitude of changes in the end-members with those of the median grain size, it is evident that during the early and middle Holocene main changes occurred primarily due to variations of EM1 and EM2 fractions. In contrast, during the last 700 yr, changes in EM3 dominantly shaped the marked decline in the median grain size.

CPD
8, 2281–2320, 2012

Assigning EM1, EM2, and EM3 to a specific transport mechanism largely relies on our understanding of modern sediment mobilization at the regional level. The grain size of present-day Namib Desert dust collected above the Walvis Ridge (Stuut et al., 2002) shows a broad uni-modal distribution with a modal value of 20 µm that is very similar to that of EM1 (Fig. 3e). Changes in wind strength and shifts of dust source throughout the investigate time interval may have had an effect on the modal value of the dust components. Based on several lines of evidence (see below), we suggest that the variability of EM1 and EM2 indicates changes in eolian input from distal and proximal sources. Grain size analysis of suspended particles collected from the main tributaries of the Orange River shows ∼10 % clay (<2 µm), ∼70 % fine silt (2–38 µm), ∼15 % coarse silt (38–63 µm), and ∼5 % sand (>63 µm) (Compton and Maake, 2007). The sand and coarse-to-medium silt fractions in the suspended matter of the Orange River are quickly trapped in the delta and prodelta, and carried away by the surface current to the northwest (Mabote, 1997; Rogers and Rau, 2006). Fine silt and coarse clay (2–7 µm) components of the Orange sediment load are transported by bottom current and deposited southeast of the Orange River mouth (Mabote, 1997; Rogers and Rau, 2006). In addition to the sediment of the Orange River, our core site also receives sediment from the Holgat River, Buffels, and Olifants rivers of the Namaqualand (Fig. 1). We hypothesize that EM3 presents a fluvial component, an assumption that is supported by the element ratios and isotope signatures shown below. Following the approach of Stuut et al. (2002, 2004), we calculated index for relative humidity (EM3/(EM1 + EM2 + EM3)) and wind strength changes (EM1/(EM1 + EM2)) throughout investigated time interval (see discussion section).

4.2 Variation of selected major elements

Down core variation of Ca/Al, K/Al, and Ti/Al intensity ratios are shown in Fig. 4. Cal/Al primarily reflects changes in biogenic carbonate and shows that carbonate productivity was relatively high between 11 500 and 6750 yr BP, followed by a continuous decline. We focus on K/Al and Ti/Al to address changes in terrigenous input and to infer possible weathering and transport mechanisms. On millennial scale, K/Al ratio shows a continuous decline starting from 11 500 to 6000 yr BP. An increasing K/Al trend is evident between 5500 and 5000 yr BP and during the last 700 yr BP. A millennial-scale trend in Ti/Al reveals increasing values from the early to middle Holocene and declining values from 6500 to 5000 yr BP as well as from 700 to 100 yr BP. Overall, millennial-scale trends in K/Al and Ti/Al ratios evolve in divergent directions, indicating different sources, weathering, or transport mechanisms. Clay mineralogical and chemical analyses of soil and suspended sediments in the catchment of the Orange River reveal that erosion products of the Karoo Supergroup series (Tertiary sedimentary rocks) are rich in illite, K-feldspar, smectite and show high K concentration (Compton and Maake, 2007). Furthermore, erosion products of the Karoo Supergroup series present the dominant fraction in the suspended sediment of the Orange River (Compton and Maake, 2007). Therefore, it is likely that episodes of elevated K/Al ratios indicate a dominance of riverine sediments originating from chemical weathering under wet conditions in the catchments. In contrast, high Ti/Al ratios mainly indicate eolian transport and physical erosion under dryer conditions (Compton and Maake, 2007). Superimposed on the millennial-scale trends, both K/Al and Ti/Al show a centennial-scale oscillation with periodicities of 1176 and 530 yr at a significance level of 95 % (not shown). These oscillations are not apparent in the Ca/Al record.

4.3 Radiogenic isotope signature of the terrigenous sediments

Sr and Nd isotope signatures of terrigenous components in marine sediments provide a useful tool to assess sediment sources and transport mechanism (Bayon et al., 2003; Grousset and Biscaye, 2005; Weldeab et al., 2002a, b, 2011; Meyer et al., 2011). We established a low-resolution time series of Sr and Nd isotopes in core GeoB8332-4. We conducted also Nd and Sr isotope analysis of suspended and river-bed sediments from the Orange River and ephemeral rivers in the coastal area (Figs. 1, 4c, d, and 5). Suspended and river-bed sediments of the Orange River that were collected at Alexander Bay and Vooldrift (Fig. 1) show average values of $^{87}Sr/^{86}Sr = 0.73224 \pm 0.0016$ ($n = 4$)

and εNd=−11.04±1.98 ($n = 4$). We note that dissolved Sr isotope values in water from the Caledon River (a tributary of the Orange River) and the Upper Orange River are much lower showing average $^{87}Sr/^{86}Sr$ values of 0.708 and 0.713, respectively (de Villiers et al., 2000). In contrast, the isotope signatures of dissolved Sr in the water of the Vaal river (also a major tributary of the Orange River) show, on average, a $^{87}Sr/^{86}Sr$ ratio of 0.731 (de Villiers et al., 2000). While more work is needed to decipher which minerals present the main source for dissolved Sr and which isotope values characterize suspended sediment loads in the main tributaries of the Orange River. Nonetheless, we argue that $^{87}Sr/^{86}Sr$ signatures of ~0.73 for suspended sediments in the Lower Orange River together with an εNd signature of = −9.19±1.45 ($n = 3$) from Beaufort Group shales which form the upper portion of the Karoo Supergroup (Dia et al., 1990) may represent integrated isotope signatures for suspended sediments of the Orange River (Fig. 5). Average values of 0.75318±0.02 ($n = 4$) and −16.9±2.05 ($n = 4$) for $^{87}Sr/^{86}Sr$ and εNd signatures characterize river-bed sediments from the local rivers (Figs. 1 and 5, Table 2). We exclude the $^{87}Sr/^{86}Sr$ and εNd values of Olifants River (Fig. 1 and Table 2) because we suspect that the sampling site is influenced by tide-mobilized sediments from the shallow water. A third sediment source is the Namib Desert dust that has an average $^{87}Sr/^{86}Sr$ and εNd value of 0.72232±0.003 ($n = 8$) and −8.64±3.24, ($n = 8$), respectively (Grousset et al., 1992).

$^{87}Sr/^{86}Sr$ and εNd values in the time series of the sediment core vary between 0.73493 and 0.719441 and −10.39 and −11.74, respectively. The down-core variation of Nd isotope values is relatively small most likely due to the dominance of Orange River sediments (Figs. 4 and 5). It is also important to note that changes in grain size have an effect on the $^{87}Sr/^{86}Sr$ signature (Eisenhauer et al., 1999; Meyer et al., 2011). Because the down core record reveals significant grain size variation (Fig. 3b), the time series of $^{87}Sr/^{86}Sr$ likely harbors an imprint of grain size changes. Therefore we emphasize that the assessment of changes in source or transport mechanism is best achieved by combining the results of all proxy parameters. Consistent with the time series of median grain size and K/Al (Figs. 3b and 4f), the radiogenic isotope signatures show a trend that is marked by decreasing $^{87}Sr/^{86}Sr$ ratios and εNd values in the early Holocene (11 600 to 9000 yr BP). During the middle Holocene, $^{87}Sr/^{86}Sr$ ratios continue to decrease until 6000 yr BP while εNd remains at a constant level similar to the end of the early Holocene (9000 yr BP). In contrast, the youngest time interval (700–0 BP) reveals increasing $^{87}Sr/^{86}Sr$ ratios and decreasing εNd values parallel to an increase in fluvial sediment supply, as suggested by the decrease in median grain-size, increase of EM3, and in the K/Al ratio (Fig. 3).

On the basis of the temporal patterns depicted in Figs. 4c, d and 5, the following relationship emerges between down-core variability of Sr and Nd isotopes and possible shifts in main sediment sources: from the early to middle Holocene, $^{87}Sr/^{86}Sr$ and εNd values decline from 0.7336 ± 0.0018 ($n = 2$) to 0.7242 ± 0.0042 ($n = 9$) and from -10.88 ± 0.11 ($n = 2$) to -11.44 ± 0.16 ($n = 9$), respectively. Concomitant increase in median grain size in the terrigenous sediments may have contributed to the relatively large decline in the $^{87}Sr/^{86}Sr$ ratio. High Ti/Al values and the dominance of EM1 with a modal grain size of ~20 µm correspond with the changes in the Sr and Nd isotopes. This suggests an enhanced influence of eolian input during the middle Holocene. From 700 yr BP toward the core top, $^{87}Sr/^{86}Sr$ and εNd reveal increasing and declining values, respectively. This trend is accompanied by changes in median grain size from coarse to fine silt and clay, an increase in the K/Al, and a decrease in Ti/Al. Changes in all parameters thus indicate increase of river sediment supply over the last 700 yr. More important, the negative trend in εNd and an increase in $^{87}Sr/^{86}Sr$ suggest a relative increase of sediment input from the local rivers.

4.4 $\delta^{18}O$ and $\delta^{13}C$ in tests of *Neogloboquadrina pachyderma* (sinistral)

The results of $\delta^{18}O$ and $\delta^{13}C$ analysis in tests of *Neogloboquadrina pachyderma* (sinistral) are shown in Fig. 4a and b. The long-term trend of the carbon isotope is marked by an increase of $\delta^{13}C$ from an average value of -1.1 ± 0.17 ($n = 55$) between 10 800 and 7000 yr BP to -0.54 ± 0.19 ($n = 21$) between 6800 and 5100 yr BP. On average, a decreasing trend in $\delta^{13}C$ is evident in the youngest section of the record (100–700 yr BP), showing a mean value of -0.18 ± 0.1 ($n = 26$).

Changes in isotope signature of dissolved inorganic carbon (DIC) and its manifestation in the carbon isotope composition of planktonic foraminiferal tests can be influenced by a multitude of processes. Due to the hydrographic, bathymetric, and depositional setting of our core site, a relatively low organic matter burial efficiency coupled with suspension and vertical mixing by bottom currents and internal waves (Compton et al., 2009), and ensuing demineralization of organic matter may present a source of DIC variability. The long-term changes in carbon isotopes, as observed in our record, however, may reflect changes in the strength of upwelling or in the amount and isotope signature of river DIC. $\delta^{13}C$ values of organic matters in soil and suspended matter in the catchment and tributaries of the Orange River cover a wide range, varying between −12.7 ‰ and −21.5 ‰ (Compton and Maake, 2007). In contrast, measurements of $\delta^{13}C$ in organic matter along a transect off the Orange River show rapidly decreasing $\delta^{13}C$ values away from riverine influenced zone, suggesting that most of the riverine organic matter is composed of C_4 plant remains and that it is deposited predominantly in the delta and prodelta systems (Meadows et al., 2002). Estimates of particulate and dissolved organic matter from the Orange River entering the delta system, on average, account for 62 000 $t\,yr^{-1}$, and half of this amount (31 000 $t\,yr^{-1}$) is buried in the subaqueous delta plains (Compton et al., 2009). Therefore, distal from the Orange River outflow, wind-induced upwelling of demineralized marine organic carbon provides the largest source of DIC. Hence, the variability of $\delta^{13}C$ in our record may serve as an indicator of changes in the strength of coastal water upwelling, with relatively low values indicating strong upwelling.

The $\delta^{18}O$ record reflects a composite imprint of changes in continental ice volume, calcification temperature, and fresh water input. We removed the ice volume component from the foraminiferal $\delta^{18}O$ record using the eustatic level record from Bard et al. (1996). A prominent feature in the ice volume corrected $\delta^{18}O$ ($\delta^{18}O_{ivc}$) record throughout the early and middle Holocene is a gradually declining trend that

CPD
8, 2281–2320, 2012

is interrupted by precipitous rises in $\delta^{18}O_{ivc}$. On multi-centennial- to millennial-scale, the ice-volume corrected $\delta^{18}O$ ($\delta^{18}O_{ivc}$) record reveals variation of 0.5‰ from the early to the middle Holocene (Fig. 5). After 7500 yr BP a gradual decline in $\delta^{18}O_{ivc}$ continued until 5000 BP, culminating in the lowest $\delta^{18}O_{ivc}$ values. Submillennial-scale change is apparent between 7500 and 5000 yr BP but not as prominent as in the earliest Holocene. Under modern climate conditions, Orange River runoff of ~11 $km^3 yr^{-1}$ is rapidly mixed with upwelled surface waters and leaves only a negligible salinity imprint in the coastal oceanic waters. It is thus likely that during the middle Holocene the decline of in the $\delta^{18}O_{ivc}$ record predominantly reflects increase in the foraminiferal calcification temperature with 0.21 ‰ °C^{-1} (Bemis et al., 1998). Parallel changes in the $\delta^{18}O$ and $\delta^{13}C$ time series during the early and middle Holocene with decreasing $\delta^{18}O$ and increasing $\delta^{13}C$ values most likely indicate millennial-scale episodes of weakened upwelling and resultant surface water warmth of approximately 2 °C (Fig. 6c and d).

5 Discussion

5.1 Early and middle Holocene climate variability

We identify two periods of millennial-scale climate changes during the early and middle Holocene. During the early Holocene (Between 11 500 and 9200 yr BP), our record reveals low dust accumulation and slightly elevated fluvial sediment input, suggesting relatively humid climate conditions in Southwestern Africa. Positive εNd values indicate a dominant contribution of the Orange River to the enhanced fluvial input (Fig. 4) that is consistent with climate record from the Tswaing Crater (Northeastern South Africa) (Kristen et al., 2010). Around 9100 yr BP, we note the onset of a continuous increase of dust mobilization and wind strength that reached its height between 6000 and 5500 yr BP (Fig. 6f). Slight changes in the Nd isotope record indicate a significant contribution of eolian particles from the Namaqualand (Fig. 4d), suggesting relatively

CPD
8, 2281–2320, 2012

arid conditions in the coastal areas of Southwestern Africa and strengthening of easterly and northeasterly winds. Increase in dust input was accompanied by a continuous weakening of coastal upwelling and surface water warming, as suggested by the $\delta^{13}C$ and $\delta^{18}O$ records (Fig. 6c and d). The observation that in the northeastern part of the Orange basin climate amelioration started at 8000 BP (Kristen et al., 2010; Holmgren et al., 2003) may indicate that our record of climate deterioration trend reflects primarily conditions in the WRZ of South Africa. At 5500 yr BP, we note a reduction in eolian sediment that is not accompanied by significant changes in the other proxy-parameters.

Comparison of our results with available terrestrial records in the WRZ in South Africa reveals a broadly consistent pattern of regional climate variability. Between 12 000 and 9500 yr BP pollen time series as well as carbon and nitrogen isotope records from the western margin of the WRZ (Meadows et al., 2010; Scott and Woodborne, 2007a, b) reveal a dominance of pollen assemblages and isotope signatures indicative of enhanced moisture availability. At ~8500 yr BP, the relatively wet conditions gave way to more arid environment that persisted until 5600 yr BP. Farther to the south within the WRZ, a $\delta^{13}C$ time series analyzed in hyrax dung also suggests early Holocene wet conditions and gradual climate deterioration throughout the middle Holocene (Fig. 6h) (Chase et al., 2011). We note that there exists a multi-centennial mismatch pertaining the onset and termination of the dry and wet phases, as reflected in the various records referred above. This mismatch could be related not only to age model uncertainties but could arise also due to the elevation and the relative proximity of the hyrax dung collection sites to the perennial rainfall zone and/or Summer Rainfall Zone (SRZ). Similarly, there exists a mismatch between the onset and termination in the strength of northeasterly and easterly winds in our record and those of dune mobilization in the coastal area (Chase and Thomas, 2006). The timing of enhanced middle Holocene dune activity along the west coast of South Africa has been constrained between 4000 and 8000 yr BP (Fig. 6g) (Chase and Thomas, 2006). Our records of dust and fluvial sedimentation indicate that the timing of dune activity in the Namaqualand overlaps to a large extent with the episode of enhanced wind strength (9000–

5500 yr BP). Chase and Thomas (2006) note that their age model most likely reflects the cessation of a dune activity rather than the onset of dune mobility. Hence, it is very likely that the onset of arid conditions, as suggested by our records, and dune mobility in the Namaqualand (Chase and Thomas, 2006) are temporally coincident and that the invigoration of the northeasterly and easterly winds was most likely critical for the dune formation. The overall picture that emerges from this comparison is a broadly consistent pattern of paleo-environmental conditions in the WRZ of Southwestern Africa with wet conditions during the early Holocene between 11 500 and 9100 yr BP and an aridification trend, gradual weakening of the Southern BUS, and surface water warming of coastal water between 9000 and 5000 yr BP.

Comparing our records with terrestrial counterparts from the southwest African summer rainfall zone (SRZ) (Chase et al., 2009, 2010) and marine records off Southwest Africa (Shi et al., 2000; Stuut et al., 2002, 2004; Stuut and Lamy, 2004), it is evident that both climate regimes indicate a trend of gradual aridification throughout the early to middle Holocene (Fig. 6e and f). On millennial and sub-millennial scales, however, there exists a significant deviation, as indicated by the return of the SRZ to humid conditions between 8700 and 7500 kyr BP (Fig. 6e) (Chase et al., 2009) and intensification of dust mobilization between 9000 and 5.5 kyr BP in the WRZ, as suggested by our record. Extending the comparison of our record to those of mid-latitude South America, we note several common features. Relatively humid conditions during the early Holocene (11.5–9.5 ± 0.5 kyr BP) and late middle Holocene centered at 5 ± 0.5 kyr BP across Southwestern Africa (Fig. 6e and h) have their counterparts in Southern South America, as indicated by rise in lake levels (Stine and Stine, 1990), dominance of moisture-indicating pollen assemblages (Moreno et al., 2010), and advance of mountain glaciers (Douglass et al., 2005). All these records suggest enhanced moisture availability, most likely in response to large-scale changes in atmospheric circulation. Key atmospheric features that exert control on the Southern Hemisphere mid-latitude moisture distribution are the westerly winds. Conceptual models emphasize that changes in the strength and latitudinal shift of the southern westerlies and

CPD
8, 2281–2320, 2012

attendant subtropical disturbances could have played a critical role in shaping past precipitation in Southwestern Africa and mid-latitude South America (Cockcroft et al., 1987; Toggweiler and Lea, 2011; Toggweiler et al., 2006; Tyson et al., 2002). Millennial- and orbital-scale climate variability in subtropical and temperate latitudes has been also linked to latitudinal shifts of the southern westerlies (Lamy et al., 2007, 2011; Moreno et al., 2010; Stuut and Lamy, 2004; Stuut et al., 2004).

A crucial observation in our record to inferring the most probable climate link and mechanism is the coupling between aridification, weakening of the Southern BUS, and surface water warming (Fig. 6). Over the same period, proxy records indicate an increase of Agulhas water leakage into Southeastern Atlantic (Peeters et al., 2004) and rise of non-sea-salt (nss) Ca^{2+} accumulation in Antarctic ice core (Roethlisberger et al., 2002) (Fig. 6a and b). An increase of the latter over Antarctica is thought to reflect an intensification and poleward shift of the austral mid-latitude westerlies (Dixon et al., 2011; Roethlisberger et al., 2002; Stager et al., 2012). Instrumental and modeling studies demonstrate that an increased leakage of warm and saline Agulhas water into the Southern Atlantic is facilitated by a southward displacement of the austral westerlies (Biastoch et al., 2008, 2009; Shannon et al., 1990). Modern observation also shows that the incursion of Agulhas water into the Southern BUS weakens the coastal upwelling and warms the surface water (Hardman-Mountford et al., 2003; Biastoch et al., 2009). Therefore, the middle Holocene dry conditions in Namaqualand and the weakening of the Southern BUS most likely occurred in response to a poleward shift of the austral westerlies and an enhanced amount of Agulhas water leakage, as suggested by geochemical analysis in Antarctic ice core (Roethlisberger et al., 2002) and shift in planktonic foraminiferal composition off South Africa (Peeters et al., 2004), respectively (Fig. 6a and b). Our combined record of terrestrial and oceanic proxies adds a robust evidence for the proposed linkage. Furthermore, we suggest that increased leakage of Agulhas water into the Southern BUS and resultant warming of the coastal water during the middle Holocene may have reduced coastal fog formation. Nowadays coastal fog formation over the cold upwelled coastal water presents an important moisture source for the flora of Namaqualand (Cowling et al., 1999; MacKellar et al., 2007). Warming of the coastal water reduces the thermal gradient between air and surface water temperature and fog formation.

5.2 Climate trend in Southwestern Africa during the "Little Ice Age"

Over the last 700 yr, the GeoB8332-3 sediment is marked by a gradual increase in fine-grained fluvial sediment (EM3). Nd and Sr isotope analyses suggest that ephemeral rivers of the Namaqualand and probably tributaries of the Lower Orange River significantly contributed to the continuous rise of fluvial sediments between 600 and 100 yr BP (Fig. 4c and d). Cave deposit in the northeastern catchment of the Orange River suggest cold and relatively dry conditions (Tyson et al., 2000). A steadily increasing flood occurrence in the banks of the Buffels River (Figs. 1 and 7j) (Benito et al., 2011) and the Lower Orange River (Herbert and Compton, 2007 and references therein) as well as pulses of freshening events evident in the Lake Verlorenvlei record (Stager et al., 2012) (Figs. 1 and 7k) over the last 700–600 yr lend credence to our Nd and Sr isotope-based inference of increased sediment contribution from the local rivers.

The increase in fluvial sediments of proximal origin between 600 and 100 yr BP falls within the time interval of global climate instability known as the "Little Ice Age" (LIA). In the Northern Hemisphere, the duration of the LIA encompasses the time between 1300 and 1850 Common Era (CE) (Holzhauser et al., 2005; Miller et al., 2012). Elsewhere, the timing of the northern cold spell is less well constrained owning to dating uncertainties and interhemispheric difference in the onset and termination of this climatic event (Schaefer et al., 2009). While anthropogenic contribution to the enhanced sediment mobilization at least during the younger part of the time series cannot be ruled out, we argue that our record largely reflects a regional expression of the global climate event associated with the LIA. Our data suggest that the winter rainfall zone of South Africa experienced continuous climate amelioration over the last 600 yr. Considering age model uncertainties that can account up to ±100 yr, the onset of humid phase in the WRZ of Southwestern Africa at 600 ± 50 yr BP is coincident with these of glacier advances in New Zealand at ∼570 yr (Schaefer et al., 2009), lake level high stand at ∼500 BP in Patagonia (Stine and Stine, 1990), dominance of wet climate-indicating pollen record from Southern South America (Moreno et al., 2010), increased precipitation in Southwestern Patagonia at around 575 yr BP (Moy et al., 2008), and the onset of increased nss Ca^{2+} accumulation of in Antarctica ice cores at ∼600 yr BP (Fig. 7a). Therefore, the increase in precipitation within the WRZ was linked to a large-scale atmospheric reorganization in mid-latitudes of the Southern Hemisphere.

The early onset of the relatively humid conditions in the WRZ is contrasted by high Ti/Al and coarse grain sizes (EM1) (Fig. 7f and g). This probably indicates that dust input remained relatively high until approximately 400 yr BP. We note that the dust source extends deep into the northern and western summer rainfall zone (SRZ) of Southwestern Africa (Prospero et al., 2002; Stuut et al., 2002), we suggest that the Ti/Al record harbors a significant imprint of the climate development in the SRZ. Consistent with our records of high Ti/Al and EM1, a δ^{15}N time series analyzed in hyrax dung located in the SRZ of Western Namibia suggests relatively dry conditions (Chase et al., 2010; Fig. 7e). Approximately at the timing of the rapid Ti/Al drop (∼400 yr BP), the δ^{15}N record (Chase et al., 2010) and reconstruction of flood deposits in Northwestern Namibia (Heine, 2004) suggest an onset of an increasingly humid episode in the SRZ. This comparison reveals that climate amelioration in the Southwestern African SRZ was delayed by ∼200 yr relative to that of the WRZ. Progressive northward expansion of the relatively wet WRZ into the southwestern margin of the SRZ presents one possible explanation. An alternative explanation arises when the timing of maximum impact of the northern LIA is considered. Intensification of ice-cap growth in the Arctic Canada (Miller et al., 2012), maximal glacier advances in Europe (Holzhauser et al., 2005), and a significantly reduced meridional heat transport to the North Atlantic (Lund and Curry, 2006) commenced between 400 and 450 yr BP. As a consequence, an increased temperature gradient between the northern mid-latitude and the tropics caused a large-scale southward displacement of the ITCZ, as suggested by the Lake

Malawi and Cariaco Basin records (Haug et al., 2001; Johnson et al., 2001). Accordingly, the alternative hypothesis could be that at 400–450 yr BP a southward displacement of the intertropical convergence zone (ITCZ) during the austral summer allowed more moisture incursion into the arid SRZ in Southwestern Africa.

Oceanic conditions off the Orange River are inferred on the basis of the $\delta^{13}C$ and $\delta^{18}O$ records analyzed in tests of *Neogloboquadrina pachyderma* (sinistral) and alkenone-based sea surface temperature (SST) estimates (Leduc et al., 2010; Meisel et al., 2011) (Fig. 7b and c). The $\delta^{13}C$ record indicates that between 700 and ~550 yr BP the Southern BUS was strengthened that was followed by a decline in upwelling and slight warming between 500 and 300 yr BP. At ~300 yr BP and intensification of the Southern BUS was established. Considering age model uncertainties, changes in SST estimates by Leduc et al. (2010) are consistent with the rise and decline of upwelling intensity, as inferred from the $\delta^{13}C$ record. The $\delta^{18}O$ record, reflecting both changes in temperature and isotopic composition of seawater, show relatively low values between 300 and 150 yr BP when $\delta^{13}C$ and SST records suggest intensified upwelling and cool surface waters. One way to reconcile this divergence is by invoking enhanced fresh water input. On multi-centennial time scale, our comparison of oceanic and terrestrial climate proxies reveals a coherent pattern between declining SST, strong upwelling off the Orange River, and humid conditions in the winter rainfall zone of Southwestern Africa, indicating a common underlying cause. More northerly position of the austral mid-latitude westerlies, as suggested by low nss Ca^{2+} accumulation rate in Antarctic ice cores (Dixon et al., 2011; Roethlisberger et al., 2002), may have facilitated relatively enhanced precipitation, reduced the amount of Agulhas leakage, and enhanced upwelling that is in line with persistently increased upwelling in our record. While our interpretation pertaining the possible role of the westerlies during the LIA is consistent with these of Stager et al. (2012), our record provide additional evidence of oceanic imprints of equatorward shifts of the westerlies.

CPD
8, 2281–2320, 2012

6 Summary and conclusion

We present a climate record of Southwestern Africa that provides detailed insights into terrestrial and oceanic environmental conditions. Grain size analysis and end-member modeling accompanied by element ratio as well as stable and radiogenic isotope measurements allow the reconstruction of dust mobilization, variations in coastal upwelling, and fluvial input from perennial and ephemeral rivers. Our proxies indicate that the middle Holocene was marked by a continuous aridification that reached its height at around 5500 yr BP. Increased dust deposition and weakening of the upwelling system are paralleled by a decreasing SE trade-wind intensity (Stuut et al., 2002; Stuut and Lamy, 2004) and enhanced leakage of warm Agulhas water (Peeters et al., 2004). We suggest that our mid Holocene dust record reflects an intensification of easterly and northeasterly winds. The coincidence of local wind intensification and dune formation along the coast area of Northwestern South Africa (Chase and Thomas, 2006) may suggest a more prominent role of the northeasterly and easterly wind strength in the formation of the dune.

Corroborating recent findings in sediment sequences of the Buffels River (Benito et al., 2011) and Lake Verlorenvlei (Stager et al., 2012), our study indicates that the coastal area of Southwestern Africa experienced increasingly wet climate conditions during the last 600 yr BP. Furthermore, the multi-proxy record provides key hints as how the SRZ have climatically evolved during the LIA. The onset of relatively humid conditions in the SRZ lags by ∼200 yr relative to that of the WRZ. The delayed onset corresponds to the timing of a significant weakening of heat export to the North Atlantic from the tropics (Lund and Curry, 2006) and a large-scale southward displacement of the ITCZ towards South Africa (Johnson et al., 2001; Haug et al., 2001). Hence, while a northward expansion of the humid WRZ into the arid SRZ can not be ruled out, a southward shift of the ITCZ may have played a more dominant role in bringing more moisture to the SRZ.

CPD
8, 2281–2320, 2012

The relatively wet phase in the WRZ during the Northern Hemisphere LIA shares many feature in common with climate records of the mid-latitude South America and New Zealand most likely indicating a common cause. Climate models point out to a critical role that a latitudinal shift of westerlies could have played in modulating past precipitation in the subtropical and mid-latitudes (Cockcroft et al., 1987; Toggweiler et al., 2006; Tyson et al., 2002). Our study provides evidence that the wet episodes in the coastal area of Southwestern Africa were accompanied by relatively strong upwellings and cold surface waters. Conversely, the middle Holocene gradual aridification trend was paralleled by a weakening of the Southern BUS. These observations are consistent with latitudinal shift of austral mid-latitude westerlies and varying amount of Agulhas water leakage into the Southern BUS.

The findings of this study highlight the linkage between terrestrial climate in the coastal area and the variability of the Southern BUS that appears to be critical toward a better understanding of the Southwestern Africa climate regime and its link to mid-latitude atmospheric and ocean circulation. Based on the temporal and most likely causal relationship between the middle Holocene dry climate conditions in the WRZ, weakening of the Southern BUS, increased leakage of warm Agulhas water, and poleward shifts of the austral mid-latitude westerlies, our findings lend a strong support to the notion that in the context of global climate change southward shifts of the westerlies may result in a weakening of precipitation in the WRZ, a decline in the upwelling intensity with implication for the phytoplankton productivity and local fishery. Furthermore, increasing leakage of Agulhas as result of water southward shift of the westerlies may cause further warming of the surface water and reduces coastal fog formation.

Acknowledgements. We thank the Capitan, Crew, and participants of R/V *Meteor Cruise* M53-6. We thank John Compton (University of Cape Town, South Africa) for providing a sediment sample from Alexander Bay, Holly Avery for help with stable isotope sample preparation, Gerrt-Jan Weltje for providing the End-Member Modeling Algorithm software. S. Weldeab is grateful to UCSB for a generous start-up package.

References

Bard, E., Hamelin, B., Arnold, M., Montaggioni, L., Cabioch, G., Faure, G., and Rougerie, F.: Deglacial sea-level record from Tahiti corals and the timing of global meltwater discharge, Nature, 382, 241–244, 1996.

Bayon, G., German, C. R., Nesbitt, R. W., Bertrand, P., and Schneider, R. R.: Increased input of circumpolar deep water-borne detritus to the glacial SE Atlantic Ocean, Geochem. Geophys. Geosy., 4, 1025, doi:10.1029/2002GC000371, 2003.

Bemis, B. E., Spero, H., Bijma, J., and Lea, D. W.: Reevaluation of oxygen isotope composition of planktonic foraminifera: experimental results and revised paleotemperature equations, Paleoceanography, 13, 150–160, 1998.

Benito, G., Thorndycraft, V. R., Rico, M. T., Sanchez-Moya, Y., Sopena, A., Botero, B. A., Machado, M. J., Davis, M., and Perez-Gonzalez, A.: Hydrological response of a dryland ephemeral river to Southern African climatic variability during the last millennium, Quaternary Res., 75, 471–482, doi:10.1016/j.yqres.2011.01.004, 2011.

Biastoch, A., Boning, C. W., and Lutjeharms, J. R. E.: Agulhas leakage dynamics affects decadal variability in Atlantic overturning circulation, Nature, 456, 489–492, doi:10.1038/nature07426, 2008.

Biastoch, A., Boning, C. W., Schwarzkopf, F. U., and Lutjeharms, J. R. E.: Increase in Agulhas leakage due to poleward shift of Southern Hemisphere westerlies, Nature, 462, 495–498, doi:10.1038/nature08519, 2009.

Bremner, J. M., Rogers, J., and Willis, J. P.: Sedimentological aspects of the 1988 Orange River flods, T. Roy. Soc. S. Afr., 47, 247–294, 1990.

Chase, B. M. and Meadows, M. E.: Late Quaternary dynamics of Southern Africa's winter rainfall zone, Earth-Sci. Rev., 84, 103–138, 2007.

Chase, B. M. and Thomas, D. S. G.: Late Quaternary dune accumulation along the western margin of South Africa: distinguishing forcing mechanisms through the analysis of migratory dune forms, Earth Planet. Sc. Lett., 251, 318–333, doi:10.1016/j.epsl.2006.09.017, 2006.

Chase, B. M. and Thomas, D. S. G.: Multiphase late Quaternary aeolian sediment accumulation in Western South Africa: timing and relationship to palaeoclimatic changes inferred from the marine record, Quatern. Int., 166, 29–41, 2007.

Chase, B. M., Meadows, M. E., Scott, L., Thomas, D. S. G., Marais, E., Sealy, J., and Reimer, P. J.: A record of rapid Holocene climate change preserved in hyrax middens from Southwestern Africa, Geology, 37, 703–706, doi:10.1130/g30053a.1, 2009.

Chase, B. M., Meadows, M. E., Carr, A. S., and Reimer, P. J.: Evidence for progressive Holocene aridification in Southern Africa recorded in Namibian hyrax middens: implications for African Monsoon dynamics and the "African Humid Period", Quaternary Res., 74, 36–45, doi:10.1016/j.yqres.2010.04.006, 2010.

Chase, B. M., Quick, L. J., Meadows, M. E., Scott, L., Thomas, D. S. G., and Reimer, P. J.: Late glacial interhemispheric climate dynamics revealed in South African hyrax middens, Geology, 39, 19–22, doi:10.1130/g31129.1, 2011.

Cockcroft, M. J., Wilkinson, M. J., and Tyson, P. D.: The application of a present-day climatic model to the late quaternary in Southern Africa, Climatic Change, 10, 161–181, doi:10.1007/bf00140253, 1987.

Compton, J. S. and Maake, L.: Source of the suspended load of the upper Orange River, South Africa, S. Afr. J. Geol., 110, 339–348, doi:10.2113/gssajg.110.2-3.339, 2007.

Compton, J. S., Herbert, C., and Schneider, R.: Organic-rich mud on the western margin of Southern Africa: nutrient source to the Southern Ocean?, Global Biogeochem. Cy., 23, GB4030, doi:10.1029/2008gb003427, 2009.

Compton, J. S., Herbert, C. T., Hoffman, M. T., Schneider, R. R., and Stuut, J.-B.: A tenfold increase in the Orange River mean Holocene mud flux: implications for soil erosion in South Africa, Holocene, 20, 115–122, doi:10.1177/0959683609348860, 2010.

Cowling, R. M., Esler, K. J., and Rundel, P. W.: Namaqualand, South Africa: an overview of a unique winter-rainfall desert ecosystem, Plant Ecol., 142, 3–21, 1999.

de Villiers, S., Compton, J. S., and Lavelle, M.: The strontium isotope systematics of the Orange River, Southern Africa, S. Afr. J. Geol., 103, 237–248, doi:10.2113/1030237, 2000.

Dia, A., Allegre, C. J., and Erlank, A. J.: The development of continental crust through geological time: the South African case, Earth Planet. Sc. Lett., 98, 74–89, 1990.

Dixon, D. A., Mayewski, P. A., Goodwin, I. D., Marshall, G. J., Freeman, R., Maasch, K. A., and Sneed, S. B.: An ice-core proxy for northerly air mass incursions into West Antarctica, Int. J. Climatol., online first: doi:10.1002/joc.2371, 2011.

Douglass, D. C., Singer, B. S., Kaplan, M. R., Ackert, R. P., Mickelson, D. M., and Caffee, M. W.: Evidence of early Holocene glacial advances in Southern South America from cosmogenic surface-exposure dating, Geology, 33, 237–240, doi:10.1130/g21144.1, 2005.

Eisenhauer, A., Meyer, H., Rachold, V., Tuetken, T., Wiegand, B., Hansen, B. T., Spielhagen, R. F., Lindemann, F., and Kassens, H.: Grain size separation and sediment mixing in Arctic Ocean sediments: evidence from the strontium isotope systematic, Chem. Geol., 158, 173–188, 1999.

Grousset, F. E. and Biscaye, P. E.: Tracing dust sources and transport patterns using Sr, Nd and Pb isotopes, Chem. Geol., 222, 149–167, 2005.

Grousset, F., Biscaye, P. E., Revel, M., and Petit, J.-R.: Antarttic (Dome C) ice-core dust at 18 kyr BP: isotopic constraints on origins, Earth Planet. Sc. Lett., 111, 175–182, 1992.

Hardman-Mountford, N. J., Richardson, A. J., Agenbag, J. J., Hagen, E., Nykjaer, L., Shillington, F. A., and Villacastin, C.: Ocean climate of the South East Atlantic observed from satellite data and wind models, Prog. Oceanogr., 59, 181–221, doi:10.1016/j.pocean.2003.10.001, 2003.

Haug, G. H., Hughen, K. A., Sigman, D. M., Peterson, L. C., and Röhl, U.: Southward migration of the intertropical convergence zone through the Holocene, Science, 293, 1304–1308, 2001.

Heine, K.: Little Ice Age climatic fluctuations in the Namib Desert, Namibia, and adjacent areas: Evidence of exceptionally large floods from slack water deposits and desert soil sequences, in: Palecology of Quaternary Drylands, edited by: Smykatz-Kloss, W. and Felix-Henningsen, P., Lecture Notes in Earth Sciences, Springer-Verlag, Springer Berlin/Heidelberg, 137–165, 2004.

Herbert, C. T. and Compton, J. S.: Geochronology of Holocene sediments on the western margin of South Africa, S. Afr. J. Geol., 110, 327–338, doi:10.2113/gssajg.110.2-3.327, 2007.

Holmgren, K., Lee-Thorp, J. A., Cooper, G. R. J., Lundblad, K., Partridge, T. C., Scott, L., Sithaldeen, R., Siep Talma, A., and Tyson, P. D.: Persistent millennial-scale climatic variability over the past 25 000 yr in Southern Africa, Quaternary Sci. Rev., 22, 2311–2326, 2003.

Holzhauser, H., Magny, M., and Zumbuhl, H. J.: Glacier and lake-level variations in west-central Europe over the last 3500 yr, Holocene, 15, 789–801, doi:10.1191/0959683605hl853ra, 2005.

Jacobson, S. B. and Wasserburg, G. J.: Sm-Nd isotopic evolution of chondrites, Earth Planet. Sc. Lett., 50, 139–155, 1980.

Johnson, T. C., Barry, S. L., Chan, Y., and Wilkinson, P.: Decadal record of climate variability spanning the past 700 yr in the Southern Tropics of East Africa, Geology, 29, 83–86, doi:10.1130/0091-7613(2001)029<0083:drocvs>2.0.co;2, 2001.

CPD

8, 2281–2320, 2012

Kreutz, K. J. and Mayewski, L. D.: Spatial variability of Antarctic surface snow glaciochemistry: implications for paleoatmospheric circulation and reconstructions, Antarct. Sci., 11, 105–118, 1999.
Kristen, I., Wilkes, H., Vieth, A., Zink, K. G., Plessen, B., Thorpe, J., Partridge, T., and Oberhänsli, H.: Biomarker and stable carbon isotope analyses of sedimentary organic matter from Lake Tswaing: evidence for deglacial wetness and early Holocene drought from South Africa, J. Paleolimnol., 44, 143–160, doi:10.1007/s10933-009-9393-9, 2010.
Lamy, F., Kaiser, J., Arz, H. W., Hebbeln, D., Ninnemann, U., Timm, O., Timmermann, A., and Toggweiler, J. R.: Modulation of the bipolar seesaw in the southeast pacific during Termination 1, Earth Planet. Sc. Lett., 259, 400–413, doi:10.1016/j.epsl.2007.04.040, 2007.
Lamy, F., Kilian, R., Arz, H. W., Francois, J.-P., Kaiser, J., Prange, M., and Steinke, T.: Holocene changes in the position and intensity of the southern westerly wind belt, Nat. Geosci., 3, 695–699, 2011.
Leduc, G., Herbert, C. T., Blanz, T., Martinez, P., and Schneider, R.: Contrasting evolution of sea surface temperature in the Benguela upwelling system under natural and anthropogenic climate forcings, Geophys. Res. Lett., 37, L20705, doi:10.1029/2010gl044353, 2010.
Lund, D. C. and Curry, W.: Florida Current surface temperature and salinity variability during the last millennium, Paleoceanography, 21, PA2009, doi:10.1029/2005pa001218, 2006.
Lutjeharms, J. R. E., Monteiro, P. M. S., Tyson, P. D., and Obura, D.: The oceans around Southern Africa and regional effects of global change, S. Afr. J. Sci., 97, 119–130, 2001.
Mabote, M. E., Rogers, J., and Meadows, M. E.: Sedimentology of terrigenous mud from the orange river delta and the inner shelf off Namaqualand, South Africa, S. Afr. Geogr. J., Special Edn., 108–114, 1997.
MacKellar, N. C., Hewitson, B. C., and Tadross, M. A.: Namaqualand's climate: Recent historical changes and future scenarios, J. Arid. Environ., 70, 604–614, 2007.
Meadows, M. E. and Sugden, J. M.: A vegetation history of the last 14 000 years on the Cederberg, South-Western Cape Province, S. Afr. J. Sci., 87, 34–43, 1991.
Meadows, M. E., Rogers, J., Lee-Thorp, J. A., Bateman, M. D., and Dingle, R. V.: Holocene geochronology of a continentalshelf mudbelt off Southwestern Africa, Holocene, 12, 59–67, doi:10.1191/0959683602hl521rp, 2002.
Meadows, M. E., Chase, B. M., and Seliane, M.: Holocene palaeoenvironments of the Cederberg and Swartruggens mountains, Western Cape, South Africa: Pollen and

CPD
8, 2281–2320, 2012

Holocene climate variability in the winter rainfall zone of South Africa

S. Weldeab et. al.

stable isotope evidence from hyrax dung middens, J. Arid. Environ., 74, 786–793, doi:10.1016/j.jaridenv.2009.04.020, 2010.

Meisel, S., Struck, U., and Emeis, K.-C.: Nutrient dynamics and oceanographic features in the Central Namibian upwelling region as reflected in δ15N-signals of suspended matter and surface sediments, Foss. Rec., 14, 153–169, doi:10.1002/mmng.201100005, 2011.

Meyer, I., Davies, G. R., and Stuut, J.-B. W.: Grain size control on Sr-Nd isotope provenance studies and impact on paleoclimate reconstructions: An example from deep-sea sediments offshore NW Africa, Geochem. Geophys. Geosy., 12, doi:10.1029/2010gc003355, 2011.

Miller, G. H., Geirsdottir, A., Zhong, Y., Larsen, D. J., Otto-Bliesner, B. L., Holland, M. M., Bailey, D. A., Refsnider, K. A., Lehman, S. J., Southon, J. R., Anderson, C., Björnsson, H., and Thordarson, T.: Abrupt onset of the Little Ice Age triggered by volcanism and sustained by sea-ice/ocean feedbacks, Geophys. Res. Lett., 39, L02708, doi:10.1029/2011GL050168, 2012.

Moreno, P. I., Francois, J. P., Moy, C. M., and Villa-Martinez, R.: Covariability of the southern westerlies and atmospheric CO_2 during the Holocene, Geology, 38, 727–730, doi:10.1130/g30962.1, 2010.

Moy, C. M., Dunbar, R. B., Moreno, P. I., Francois, J. P., Villa-Martinez, R., Mucciarone, D. M., Guilderson, T. P., and Garreaud, R. D.: Isotopic evidence for hydrologic change related to the westerlies in SW Patagonia, Chile, during the last millennium, Quaternary Sci. Rev., 27, 1335–1349, doi:10.1016/j.quascirev.2008.03.006, 2008.

Peeters, F. J. C., Acheson, R., Brummer, G. J. A., de Ruijter, W. P. M., Schneider, R. R., Ganssen, G. M., Ufkes, E., and Kroon, D.: Vigorous exchange between the Indian and Atlantic oceans at the end of the past five glacial periods, Nature, 430, 661–665, doi:10.1038/nature02785, 2004.

Prins, M., Postma, G., and Weltje, G. J.: Controls on terrigenous sediment supply to the Arabian Sea during the late Quaternary: the Makran continental slope, Mar. Geol., 169, 351–371, 10.1016/s0025-3227(00)00087-6, 2000.

Prospero, J. M., Ginoux, P., Torres, O., Nicholson, S. E., and Gill, T. E.: Environmental characterization of global sources of atmospheric soil dust identified with the NIMBUS 7 Total Ozone Mapping Spectrometer (TOMS) absorbing aerosol product, Rev. Geophys., 40, 1002, doi:10.1029/2000rg000095, 2002.

Reimer, P. J., Baillie, M. G. L., Bard, E., Bayliss, A., Beck, J. W., Blackwell, P. G., Ramsey, C. B., Buck, C. E., Burr, G. S., Edwards, R. L., Friedrich, M., Grootes, P. M., Guilderson, T. P., Hajdas, I., Heaton, T. J., Hogg, A. G., Hughen, K. A., Kaiser, K. F., Kromer, B., McCormac, F. G., Manning, S. W., Reimer, R. W., Richards, D. A., Southon, J. R., Talamo, S., Turney, C. S. M., van der Plicht, J., and Weyhenmeye, C. E.: Intcal09 and Marine09 radiocarbon age calibration curves, 0–50 000 yr cal BP, Radiocarbon, 51, 1111–1150, 2009.

Roethlisberger, R., Mulvaney, R., Wolff, E. W., Hutterli, M. A., Bigler, M., Sommer, S., and Jouzel, J.: Dust and sea salt variability in Central East Antarctica (Dome C) over the last 45 kyr and its implications for southern high-latitude climate, Geophys. Res. Lett., 29, 1963, doi:10.1029/2002gl015186, 2002.

Rogers, J. and Rau, A. J.: Surficial sediments of the wave-dominated Orange River Delta and the adjacent continental margin off South-Western Africa, Afr. J. Mar. Sci., 28, 511–524, doi:10.2989/18142320609504202, 2006.

Schaefer, J. M., Denton, G. H., Kaplan, M., Putnam, A., Finkel, R. C., Barrell, D. J. A., Andersen, B. G., Schwartz, R., Mackintosh, A., Chinn, T., and Schlüchter, C.: High-frequency Holocene glacier fluctuations in New Zealand differ from the northern signature, Science, 324, 622–625, doi:10.1126/science.1169312, 2009.

Scott, L. and Woodborne, S.: Vegetation history inferred from pollen in Late Quaternary faecal deposits (hyraceum) in the Cape winter-rain region and its bearing on past climates in South Africa, Quaternary Sci. Rev., 26, 941–953, doi:10.1016/j.quascirev.2006.12.012, 2007a.

Scott, L. and Woodborne, S.: Pollen analysis and dating of Late Quaternary faecal deposits (hyraceum) in the Cederberg, Western Cape, South Africa, Rev. Palaeobot. Palyno., 144, 123–134, doi:10.1016/j.revpalbo.2006.07.004, 2007b.

Shannon, L. V., Agenbag, J. J., Walker, N. D., and Lutjeharms, J. R. E.: A major perturbation in the Agulhas retroflection area in 1986, Deep-Sea Res. Pt. I, 37, 493–512, doi:10.1016/0198-0149(90)90021-m, 1990.

Shi, N., Dupont, L. M., Beug, H.-J. r., and Schneider, R.: Correlation between Vegetation in Southwestern Africa and oceanic upwelling in the past 21 000 yr, Quaternary Res., 54, 72–80, 2000.

Stager, J. C., Mayewski, P. A., White, J., Chase, B. M., Neumann, F. H., Meadows, M. E., King, C. D., and Dixon, D. A.: Precipitation variability in the winter rainfall zone of South Africa during the last 1400 yr linked to the austral westerlies, Clim. Past, 8, 877–887, doi:10.5194/cp-8-877-2012, 2012.

Stine, S. and Stine, M.: A record from Lake Cardiel of climate change in Southern South-America, Nature, 345, 705–708, doi:10.1038/345705a0, 1990.

Stuiver, M. and Reimer, P. J.: Extended ^{14}C data-base and revised calib 3.0 C-14 age calibration program, Radiocarbon, 35, 215–230, 1993.
Stuut, J. B. W. and Lamy, F.: Climate variability at the southern boundaries of the Namib (Southwestern Africa) and Atacama (Northern Chile) coastal deserts during the last 120 000 yr, Quaternary Res., 62, 301–309, doi:10.1016/j.yqres.2004.08.001, 2004.
Stuut, J.-B. W., Prins, M. A., Schneider, R. R., Weltje, G. J., Jansen, J. H. F., and Postma, G.: A 300-kyr record of aridity and wind strength in Southwestern Africa: inferences from grain-size distributions of sediments on Walvis Ridge, SE Atlantic, Mar. Geol., 180, 221–233, 2002.
Stuut, J.-B. W., Crosta, X., van der Borg, K., and Schneider, R. R.: Relationship between Antarctic sea ice and southwest African climate during the Late Quaternary, Geology, 32, 909–912, doi:10.1130/G20709.1, 2004.
Toggweiler, J. R. and Lea, D. W.: Temperature differences between the hemispheres and ice age climate variability, Paleoceanography, 25, PA2212, doi:10.1029/2009pa001758, 2011.
Toggweiler, J. R., Russell, J. L., and Carson, S. R.: Midlatitude westerlies, atmospheric CO_2, and climate change during the ice ages, Paleoceanography, 21, doi:10.1029/2005pa001154, 2006.
Tyson, P. D., Karlen, W., Holmgren, K., and Heiss, G. A.: The Little Ice Age and medieval warming in South Africa, S. Afr. J. Sci., 96, 121–126, 2000.
Tyson, P. D., Lee-Thorp, J., Holmgren, K., and Thackeray, J. F.: Changing gradients of climate change in Southern Africa during the past millennium: Implications for population movements, Climatic Change, 52, 129–135, doi:10.1023/a:1013099104598, 2002.
Weldeab, S., Emeis, K.-C., Hemleben, C., Schulz, H., and Vennemann, T. W.: Sr, Nd isotope composition of Late Pleistocene sapropels and non-sapropel sediments from the Eastern Mediterranean Sea: Implications for detrital influx and climatic conditions in the source areas, Geochim. Cosmochim. Ac., 66, 3585–3598, 2002a.
Weldeab, S., Emeis, K.-C., Hemleben, C., and Siebel, W.: Provenance of lithogenic surface sediments and path ways of riverine suspended matters in the Eastern Mediterranean Sea: Evidence from $^{143}Nd/^{144}Nd$ and $^{87}Sr/^{86}Sr$ ratios, Chem. Geol., 186, 139–149, 2002b.
Weldeab, S., Frank, M., Stichel, T., Haley, B., and Sangen, M.: Spatio-temporal evolution of the West African monsoon during the last deglaciation, Geophys. Res. Lett., 38, L13703, doi:10.1029/2011gl047805, 2011.
Weltje, G. J.: End-member modeling of compositional data: numerical-statistical algorithms for solving the explicit mixing problem, Math. Geol., 29, 503–549, 1997.

CPD
8, 2281–2320, 2012

Table 1. Details of the material used to establish an age model for GeoB8332-4. ^{14}C ages were converted to calendar ages using CALIB software (Stuiver and Reimer, 1993) (version 6.10), Marine data set 2009 (Reimer et al., 2009), and ΔR of 129 ± 19 based on reservoir age of Southeastern Atlantic water (Sealy et al., 2012, data retrieved from http://calib.qub.ac.uk/marine as of 5 May 2012). The final age models were established using polynomial (11 500–5000 yr BP) and linear (0–700 yr BP) equations.

Lab Code	Core	Core depth (cm)	Material	^{14}C age yr BP	Cal age yr BP (median probability)	95.4 % (2σ) cal age (yr BP) ranges	Relative area under distribution	Calibration data
KIA24630	GeoB8332-4	2	gastroods	−220 ± 30	0	0		Reimer et al. (2009)
KIA25048	GeoB8332-4	50	gastroods	710 ± 25	219	124–291	1	Reimer et al. (2009)
KIA25049	GeoB8332-4	145	gastroods	1295 ± 30	709	647–784	1	Reimer et al. (2009)
KIA25834	GeoB8332-4	190	gastroods	4910 ± 35	5049	4896–5229	1	Reimer et al. (2009)
KIA25833	GeoB8332-4	220	gastroods	5290 ± 35	5525	5438–5600	1	Reimer et al. (2009)
KIA25050	GeoB8332-4	240	gastroods	5620 ± 35	5874	5746–5965	1	Reimer et al. (2009)
KIA24623	GeoB8332-4	319.5	gastroods	6730 ± 90	7115	6888–7313	1	Reimer et al. (2009)
KIA25052	GeoB8332-4	400	gastroods	7530 ± 40	7868	7759–7927	1	Reimer et al. (2009)
KIA25053	GeoB8332-4	489	gastroods	8625 ± 40	9121	8999–9257	1	Reimer et al. (2009)
KIA25057	GeoB8332-4	608	gastroods	9400 ± 50	10 109	9917–10 217	1	Reimer et al. (2009)
KIA25056	GeoB8332-4	699	gastroods	9840 ± 50	10 568	10 466–10 703	1	Reimer et al. (2009)
KIA25055	GeoB8332-4	789	gastroods	10 380 ± 85	11 253	11 102–11 445	0.9	Reimer et al. (2009)
						11 460–11 630	0.1	Reimer et al. (2009)
KIA24622	GeoB8332-4	789.5	gastroods	10 440 ± 50	11 290	11 177–11 428	0.91	Reimer et al. (2009)
						11 487–11 617	0.09	Reimer et al. (2009)
KIA25059	GeoB8332-4	805	gastroods	10 485 ± 50	11 357	11 214–11 649	1	Reimer et al. (2009)

CPD
8, 2281–2320, 2012

Table 2. Results of Sr and Nd isotope analysis in river and marine core sediments.

River samples										
Sample colde	Location	Locarion	Material	size fraction	$^{87}Sr/^{86}Sr$	$\pm^{87}Sr/^{86}Sr$	$^{143}Nd/^{144}Nd$	$\pm^{143}Nd/^{144}Nd$	εNd	Error εNd (2σ)
SP-B1	Buffels River	29°41.97′ S/17°42.75′ E	riverine mud	<125 µm	0.76760	0.00001	0.51170	0.00001	−18.20	0.12
SP-B2	Buffels River	29°36.79′ S/17°31.45′ E	riverine mud	<125 µm	0.75528	0.00001	0.51176	0.00001	−17.05	0.12
SP-FB	Dry river bed	28°47.94′ S/17°39.06′ E	riverine mud	<125 µm	0.76666	0.00001	0.51169	0.00001	−18.41	0.12
SP-OL	Olifants Rivers	31°40.76′ S/18°11.98′ E	riverine mud	<125 µm	0.72423	0.00001	0.51207	0.00001	−11.12	0.12
SP-H	Holgat River	28°55.86′ S/16°46.44′ E	riverine mud	<125 µm	0.72320	0.00001	0.51192	0.00001	−13.97	0.12
B005	Orange River (Alexander Bay)	28°36.07′ S/16°28′16 E	riverine mud	>2 µm	0.735538	0.000001	0.512032	0.000007	−11.78	0.14
SF-OR	Orange River (Voolsdrif)	28°46.41′ S/17°38′63 E	riverine suspended matter	<20 µm	0.733628	0.000001	0.512015	0.000007	−12.11	0.14
"Alagae"	Orange River (Voolsdrif)	28°36.07′ S/16°28′16 E	riverine suspended matter	>2 µm	0.732447	0.000001	0.511991	0.000009	−12.58	0.18
SP-OR1	Orange River (Voolsdrif)	28°46.41′ S/17°38′63 E	riverine mud	<120 µm	0.727351	0.000027	0.511956	0.000008	−13.26	0.16
GeoB8332-4 samples										
Core	Sediment depth (cm)	Cal age (yr BP)	Material	Size fraction	$^{87}Sr/^{86}Sr$	$\pm^{87}Sr/^{86}Sr$	$^{143}Nd/^{144}Nd$	$\pm^{143}Nd/^{144}Nd$	εNd	Error εNd (2σ)
GeoB8332-4	2	0	Terrigenous fraction	<125 µm	0.734426	0.000009	0.512066	0.000008	−11.12	0.16
GeoB8332-4	35	157.2	Terrigenous fraction	<125 µm	0.734077	0.000008	0.512081	0.000009	−10.83	0.18
GeoB8332-4	102.5	493.6	Terrigenous fraction	<125 µm	0.729606	0.000008	0.512103	0.000010	−10.40	0.20
GeoB8332-4	180	879.8	Terrigenous fraction	<125 µm	0.721613	0.00001	0.512047	0.000007	−11.49	0.14
GeoB8332-4	230	5736.7	Terrigenous fraction	<125 µm	0.721173	0.00001	0.512052	0.000010	−11.39	0.20
GeoB8332-4	285	6551.2	Terrigenous fraction	<125 µm	0.719441	0.00001	0.512045	0.000009	−11.53	0.18
GeoB8332-4	315	6972.6	Terrigenous fraction	<125 µm	0.721116	0.000009	0.512049	0.000010	−11.45	0.20
GeoB8332-4	385	7892.7	Terrigenous fraction	<125 µm	0.72176	0.00001	0.512064	0.000010	−11.16	0.20
GeoB8332-4	445	8611.2	Terrigenous fraction	<125 µm	0.724198	0.000007	0.512047	0.000010	−11.49	0.20
GeoB8332-4	470	8891.5	Terrigenous fraction	<125 µm	0.724615	0.000009	0.512047	0.000007	−11.49	0.14
GeoB8332-4	485	9054.2	Terrigenous fraction	<125 µm	0.725862	0.00001	0.512034	0.000009	−11.74	0.18
GeoB8332-4	552.5	9736.5	Terrigenous fraction	<125 µm	0.731262	0.000008	0.512051	0.000009	−11.41	0.18
GeoB8332-4	662.5	10 672.6	Terrigenous fraction	<125 µm	0.731666	0.000009	0.51206	0.000009	−11.24	0.18
GeoB8332-4	745	11 231.7	Terrigenous fraction	<125 µm	0.732319	0.00001	0.512082	0.000009	−10.81	0.18
GeoB8332-4	775	11 404.7	Terrigenous fraction	<125 µm	0.73493	0.000008	0.512074	0.000005	−10.96	0.10

CPD
8, 2281–2320, 2012

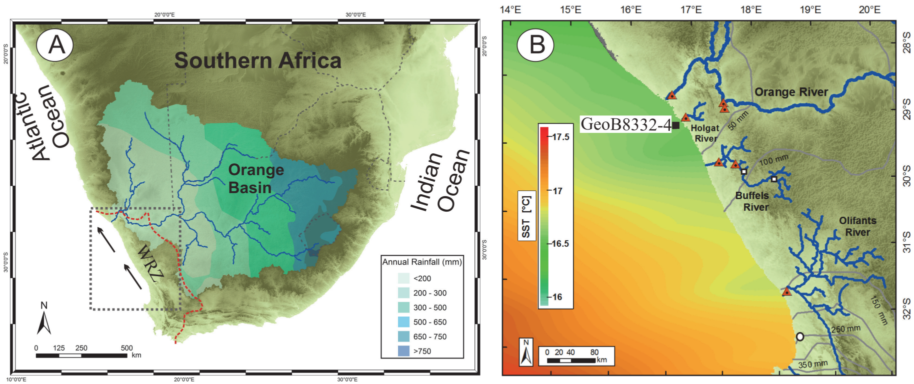

Fig. 1. (A) Map of Southern Africa indicating the basin of the Orange River, annual rainfall over the basin (rainfall contour redrawn from Compton et al., 2010), and the Winter Rainfall Zone (WRZ) delineated by the orange line. Black arrows indicate southeasterly trade winds. Dotted square indicate area whose details is shown in **(B)**. **(B)** Coastal area of Southwestern Africa showing local rivers, annual precipitation (gray contours), annual sea surface temperature (Locarnini et al., 2010), location of GeoB8332-4 (black square), and riverine sediment samples used for Sr and Nd isotope analyses (orange triangles). Shown is also the approximate location of Lake Verlorenvlei (white circle) (Stager et al., 2012) and paleo-flood investigation on the Buffels River banks (white squares) (Benito et al., 2011).

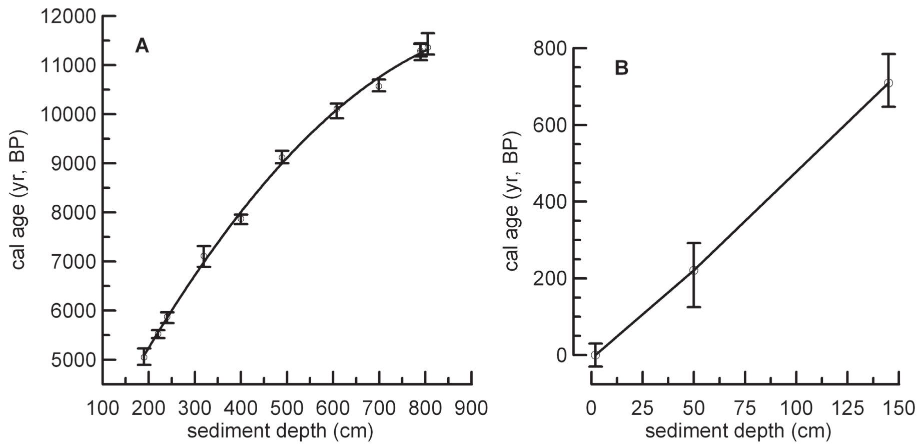

Fig. 2. Calendar age versus GeoB8332-1 sediment depth. Open circles, vertical bars, and lines indicate ^{14}C-based age model control points, uncertainty in the age model control points (2σ), and the final age model that is based on polynomial **(A)** and linear fits **(B)**.

CPD
8, 2281–2320, 2012

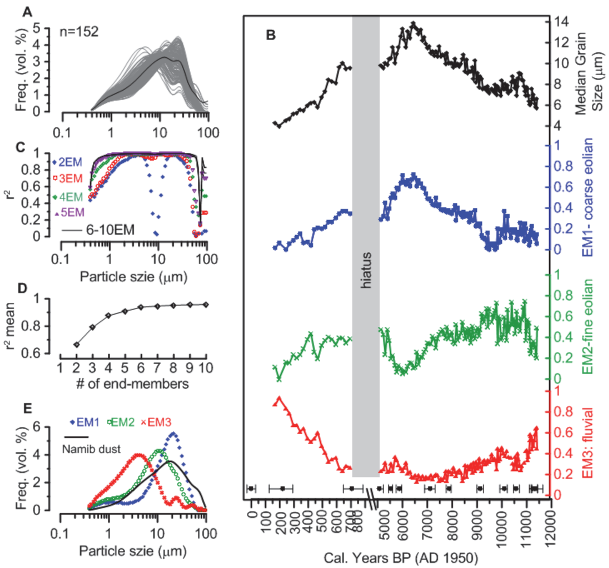

Fig. 3. Results of grain size analysis and end-member modeling for core GeoB8332-4 material. **(A)** Grain size distribution frequency for 152 samples (grey lines) and average grain size distribution frequency for the entire data set (black line). **(B)** Temporal distribution of median grain size and modeled end-members 1–3, indicating coarse eolian (EM1), fine eolian (EM2), and fluvial (EM3) components. Black filled circles and horizontal bars indicate age model control points and error estimate (2σ) obtained from ^{14}C datings and conversion to calendar age. **(C)** r^2 goodness-of-fit of models with 2–10 end-members for each particle size class. **(D)** r^2 mean (mean coefficient of determination) of all size classes for each end-member model. **(E)** Comparison of particle size distributions in EM1, EM2, and EM3 with present-day dust collected over the Walvis Ridge (Stuut et al., 2002).

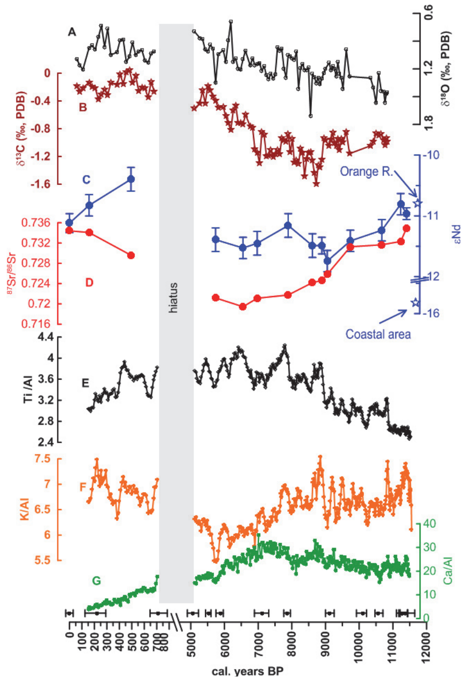

Fig. 4. Proxy time series analyzed in sediment core GeoB8332-4. **(A)** and **(B)** $\delta^{18}O$ and $\delta^{13}C$ analyzed in tests of *N. pachyderma* (sinistral). **(C)** and **(D)** εNd and $^{87}Sr/^{86}Sr$ analyzed in the detrital fraction. Average εNd value of Orange River and river-bed sediments from the coastal area indicated by stars in the y-axis. Vertical bars indicate analytical error estimates for εNd. Analytical error estimate for $^{87}Sr/^{86}Sr$ is smaller than the dots indicating individual measurements. Ti/Al **(E)**, K/Al **(F)**, and Ca/Al **(G)** analyzed in bulk sediment of GeoB8332-4 using XRF-Scanning. Black filled circles and horizontal bars indicate age model control points and error estimate (2σ) related to ^{14}C measurements and conversion to calendar age, respectively.

CPD
8, 2281–2320, 2012

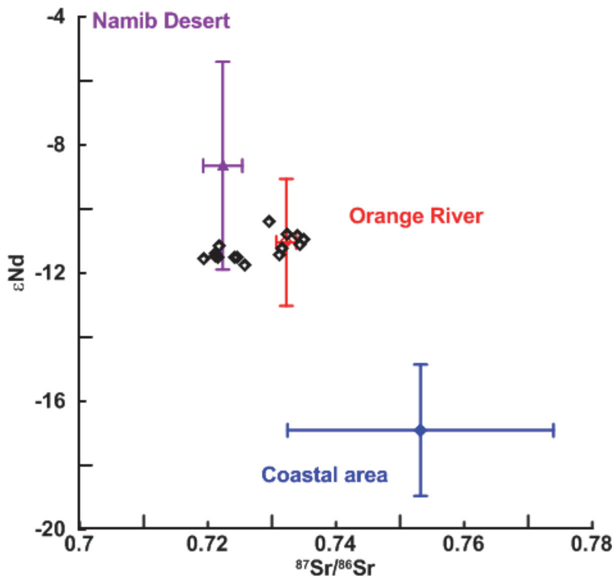

Fig. 5. Sr and Nd isotope signatures of the main sediment sources and temporal variation in sediment core GeoB8332-4 (open diamonds). Mean and εNd values and standard deviations of Namib Desert dust (^{87}Sr/^{86}Sr=0.722 ± 0.003 and εNd=−8.65 ± 3.24, $n = 6$) (Grousset et al., 1992), sediment of coastal area (^{87}Sr/^{86}Sr=0.75318 ± 0.02 and εNd=−16.9 ± 2.05, $n = 2$), Orange River sediments collected at Alexander Bay and Vooldrift (see Fig. 1) and main catchment of Orange River (Dia et al., 1990) (^{87}Sr/^{86}Sr=0.7322 ± 0.0015, $n = 4$ and εNd=−11.04 ± 1.98, $n = 6$).

CPD
8, 2281–2320, 2012

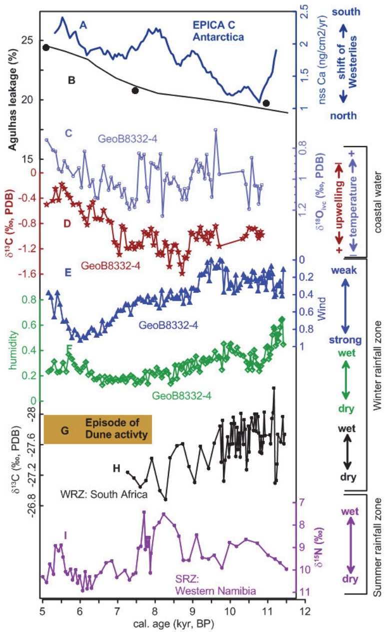

Fig. 6. Early and middle Holocene paleo-environmental proxies reconstructed from climate archives in Southwestern Africa and Antarctica. **(A)** 7 point-running average of nss Ca^{2+} analyzed in EPICA Dome C ice core indicating variation of dust incursion over Antarctica in response to latitudinal shifts if the austral westerlies (Roethlisberger et al., 2002). **(B)** Estimate of Agulhas leakage into the Southern Atlantic (Peeters et al., 2004). **(C)** Ice-volume corrected $\delta^{18}O$ ($\delta^{18}O_{ivc}$) and **(D)** $\delta^{13}C$ analyzed in *N. pachyderma* (sinistral) in core GeoB8332-4. **(E)** Wind strength ([EM1/(EM1 + EM2)]) and **(F)** humidity ([EM3/(EM1 + EM2 + EM3)]) indices inferred from grain size analysis and end-member modeling from the lithogenic fraction in GeoB8332-4. **(G)** Orange box indicates time interval (8–4 kyr BP) of enhanced dune activity in the coastal area of Southwestern Africa (Chase and Thomas, 2006). **(H)** $\delta^{13}C$ and **(I)** $\delta^{15}N$ analyzed in hyrax dung from the WRZ in South Africa (Chase et al., 2011) and the SRZ in Western Namibia (Chase et al., 2009), respectively.

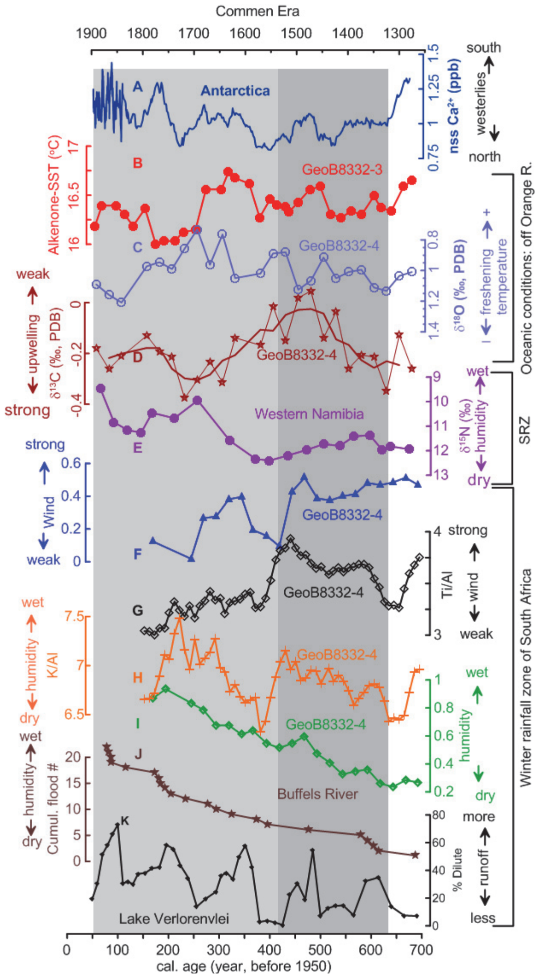

Fig. 7. Caption on next page.

CPD
8, 2281–2320, 2012

Holocene climate variability in the winter rainfall zone of South Africa

S. Weldeab et. al.

Title Page
Abstract | Introduction
Conclusions | References
Tables | Figures
◀| |▶
◀ ▶
Back | Close
Full Screen / Esc
Printer-friendly Version
Interactive Discussion

Fig. 7. Environmental conditions during the "Little Ice Age" in Southwestern Africa. **(A)** 21-points running average of non-sea-salt Ca^{2+} (nss Ca^{2+}=Na−0.038 Ca^{2+}) analyzed in Antarctic ice core (Siple Dom) (Kreutz and Mayewski, 1999). **(B)** Alkenone-based SST estimates off Holgat River analyzed in GeoB8332-3 (Leduc et al., 2010). Note that the locations of GeoB8332-3 and GeoB8332-4 are identical. **(C)** $\delta^{18}O$ and **(D)** $\delta^{13}C$ analyzed in *N. pachyderma* (sinistral) in core GeoB8332-4. **(E)** $\delta^{15}N$ analyzed in hyrax dung from the SRZ in Western Namibia (Chase et al., 2009). **(F)** Wind strength inferred from grain size analyses and modeling in core GeoB8332-4. **(G)** Ti/Al and **(H)** K/Al analyzed in core GeoB8332-4. **(I)** Humidity index inferred from grain size analyses and modeling in core GeoB8332-4. **(J)** Cumulative flood number over the last 700 yr BP reconstructed in Buffels River banks (Benito et al., 2011). **(K)** Percentage of diatom assemblage that are indicative for enhanced runoff in Lake Verlorenvlei (Stager et al., 2012). Dark grey area indicates time interval when fluvial proxies suggest wet conditions, high dust input, and strong winds in the WRZ. Light grey area indicates episode of wet conditions in both WRZ and SRZ.

CPD
8, 2281–2320, 2012